

THE LONGEST PERIOD *TESS* PLANET YET: A SUB-NEPTUNE TRANSITING A BRIGHT, NEARBY K DWARF STAR

DIANA DRAGOMIR^{1,2}, JOHANNA TESKE^{2,3,4}, MAXIMILIAN N. GÜNTHER^{1,5}, DAMIEN SÉGRANSAN⁶, JENNIFER A. BURT^{1,5}, CHELSEA X. HUANG^{1,5}, ANDREW VANDERBURG^{7,8}, ELISABETH MATTHEWS¹, XAVIER DUMUSQUE⁶, KEIVAN G. STASSUN⁹, JOSHUA PEPPER¹⁰, GEORGE R. RICKER¹, ROLAND VANDERSPEK¹, DAVID W. LATHAM¹¹, SARA SEAGER^{1,12,13}, JOSHUA N. WINN¹⁴, JON M. JENKINS¹⁵, THOMAS BEATTY^{16,17}, FRANÇOIS BOUCHY⁶, R. PAUL BUTLER³, JEFFREY D. CRANE⁴, JASON D. EASTMAN¹¹, JIM FRANCIS¹, B. SCOTT GAUDI¹⁸, ROBERT F. GOEKE¹, DAVID JAMES¹¹, TODD C. KLAUS¹⁹, RUDOLF B. KUHN^{20,21}, CHRISTOPHE LOVIS⁶, MICHAEL B. LUND⁹, SCOTT McDERMOTT²², MARTIN PAEGERT¹¹, FRANCESCO PEPE⁶, JOSEPH E. RODRIGUEZ¹¹, LIZHOU SHA¹, STEPHEN A. SHECTMAN⁴, ROBERT J. SIVERD⁹, AYLIN GARCIA SOTO¹, DANIEL J. STEVENS^{16,17}, IAN B. THOMPSON⁴, JOSEPH D. TWICKEN²³, STÉPHANE UDRY⁶, STEVEN VILLANUEVA JR.¹, SHARON X. WANG³, BILL WOHLER²³, XINYU YAO¹⁰, ZHUCHANG ZHAN^{1,12}, AND THE *TESS* TEAM

¹Department of Physics and Kavli Institute for Astrophysics and Space Research, Massachusetts Institute of Technology, Cambridge, MA 02139, USA

²NASA Hubble Fellow

³Department of Terrestrial Magnetism, Carnegie Institution for Science, 5241 Broad Branch Road, NW, Washington, DC 20015, USA

⁴Observatories of the Carnegie Institution for Science, 813 Santa Barbara Street, Pasadena, CA 91101, USA

⁵Juan Carlos Torres Fellow

⁶Astronomy Department of the University of Geneva, 51 chemin des Maillettes, 1290 Versoix, Switzerland

⁷Department of Astronomy, The University of Texas at Austin, Austin, TX 78712, USA

⁸NASA Sagan Fellow

⁹Department of Physics & Astronomy, Vanderbilt University, 6301 Stevenson Center Ln., Nashville, TN 37235, USA

¹⁰Department of Physics, Lehigh University, 16 Memorial Drive East, Bethlehem, PA 18015, USA

¹¹Center for Astrophysics | Harvard & Smithsonian, 60 Garden Street, Cambridge, MA 02138, USA

¹²Department of Earth, Atmospheric and Planetary Sciences, MIT, 77 Massachusetts Avenue, Cambridge, MA 02139, USA

¹³Department of Aeronautics and Astronautics, MIT, 77 Massachusetts Avenue, Cambridge, MA 02139, USA

¹⁴Department of Astrophysical Sciences, Princeton University, 4 Ivy Lane, Princeton, NJ 08544, USA

¹⁵NASA Ames Research Center, Moffett Field, CA, 94035, USA

¹⁶Department of Astronomy & Astrophysics, The Pennsylvania State University, 525 Davey Lab, University Park, PA 16802, USA

¹⁷Center for Exoplanets and Habitable Worlds, The Pennsylvania State University, 525 Davey Lab, University Park, PA 16802, USA

¹⁸The Ohio State University, Department of Astronomy, Columbus, OH 43210, USA

¹⁹Stinger Ghaffarian Technologies, Moffett Field, CA, 94035, USA

²⁰South African Astronomical Observatory, PO Box 9, Observatory, 7935, Cape Town, South Africa

²¹Southern African Large Telescope, PO Box 9, Observatory, 7935, Cape Town, South Africa

²²Proto-Logic LLC, 1718 Euclid Street NW, Washington, DC 20009, USA

²³SETI Institute, Mountain View, CA 94043, USA

ABSTRACT

The future of exoplanet science is bright, as *TESS* once again demonstrates with the discovery of its longest-period confirmed planet yet, located only 16 pc away. We hereby present HD 21749b (TOI 186.01), a sub-Neptune in a 36-day orbit around a bright ($V = 8.1$), nearby K4.5 dwarf. *TESS* measures HD21749b to be $2.84^{+0.26}_{-0.22} R_{\oplus}$, and combined archival and follow-up precision radial velocity data put the mass of the planet at $23.20^{+2.13}_{-1.91} M_{\oplus}$. HD 21749b is the longest-period *TESS* planet confirmed to date, and contributes to the *TESS* Level 1 Science Requirement of providing 50 transiting planets smaller than $4 R_{\oplus}$ with measured masses. Furthermore, we report the discovery of TOI 186.02, a planet candidate with a 7.8-day period which, if confirmed, could become the first Earth-sized planet discovered by *TESS*. The HD21749 system is thus a prime candidate for comparative studies of planetary composition and architecture in multi-planet systems.

Keywords: surveys: *TESS*, planetary systems, planets and satellites: detection, stars: individual (HD

21749)

1. INTRODUCTION

Small exoplanets are common in the Milky Way (Lavis et al. 2009; Howard et al. 2012; Fressin et al. 2013; Fulton et al. 2017), but for a long time astronomers have had an incomplete picture of their properties. The recently-launched Transiting Exoplanet Survey Satellite (*TESS*) is revolutionizing the field of exoplanet science by discovering planets (of all sizes) around the nearest stars. The mass, atmospheric composition and other previously mostly inaccessible properties of small exoplanets will be measurable for many *TESS* systems.

Two *TESS*-discovered planets smaller than Neptune have already been confirmed and announced. π Men b is a $2 R_{\oplus}$ super-Earth transiting its naked-eye G0V star every 6.3 days (Huang et al. 2018b). Since its mass is measured, π Men b contributes toward the *TESS* Level 1 Science Requirement of providing 50 transiting planets smaller than $4 R_{\oplus}$ with measured masses (Ricker et al. 2015). LHS 3844b is a $1.3 R_{\oplus}$ hot terrestrial planet, orbiting its star every 11 hours (Vanderspek et al. 2018). Both discoveries are based on only 27 days of *TESS* data, suggesting many more are to be expected.

Longer-period transiting planets are notoriously difficult to find because their transit probability is lower and even if they do transit, they do so more rarely. We know of very few around nearby stars. Only three small ($R_p < 4 R_{\oplus}$) planets with measured masses are known to transit stars brighter than $V=10$ and have periods > 5 days: π Men b, HD 219134c (Gillon et al. 2017) and HD 97658b (Dragomir et al. 2013), the latter having the longest period of the three, at 9.5 days. Most of the exoplanets that *TESS* will reveal will have orbital periods shorter than 10 days (Sullivan et al. 2015; Barclay et al. 2018; Huang et al. 2018a). In most parts of the sky *TESS* may only observe one or two transits for longer-period planets (Villanueva et al. 2018), making them more challenging to detect and confirm, particularly for small planets.

In this Letter we present HD 21749b (*TESS* Object of Interest 186.01), a sub-Neptune transiting exoplanet with a period of 35.61 days that initially appeared as a single-transit planet candidate. We also introduce a new planet candidate in the same system, with a period of 7.8 days. The host star is a bright ($V = 8.1$) K dwarf, located only 16 pc away, making this system likely to satisfy the follow-up interests of many exoplanet astronomers. In section 2 we describe the *TESS* photometry and the other observations (most fortuitously

acquired prior to the start of the *TESS* mission) used to confirm HD 21749b. In section 3 we describe our analysis and results. We discuss the implications of our findings and conclude in Section 4.

2. OBSERVATIONS

2.1. *TESS* Photometry

TESS will survey nearly the entire sky over two years by monitoring contiguous overlapping $90 \times 24^\circ$ sectors of the sky for 27 days at a time (Ricker et al. 2015). The primary mission will complete the southern ecliptic hemisphere in its first year, and the northern hemisphere in its second. HD 21749 has a high ecliptic latitude and was observed by *TESS* for four sectors. We use all the publicly available *TESS* data (sectors 1, 2 and 3) in our analysis, ranging from July 25 to October 14, 2018.

The first transit of HD 21749b was identified by both the MIT Quick Look Pipeline (which searches for planet candidates in the 30-min Full Frame Images) and the Science Processing Operations Center (SPOC) pipeline based at the NASA Ames Research Center (Jenkins et al. 2010, 2016; Jenkins 2017). No other matching transits were found in the publicly-released data from sectors 1 and 2. After TOI 186.01 was alerted, we searched for archival spectroscopy of this very bright star and found 59 HARPS radial velocities (RVs) in the ESO archive (see 2.3). A periodogram of these RVs showed a clear signal at 35.57 days, but the *TESS* photometry and the R_{HK} index (Boro Saikia et al. 2018) indicate a stellar rotation period around 35 days, calling for caution. If the strongest period in the RVs did indeed correspond to the planet, then we expected to see a second transit in sector 3. Once the sector 3 data were released, we discovered that a momentum dump (which causes a brief interruption in fine attitude control; Huang et al. 2018b) occurred approximately 35.6 days after the sector 1 transit (see Figure 1). We did not let this unexpected turn of events foil our search efforts, and upon close inspection of the light curve we succeeded in recovering a partial transit (including egress) immediately following the momentum dump. We found consistent depths and egress durations between the two events. The transit- and RV-derived periods agree as well (see 3.2). Serendipitously, when applied to the three-sector data, the SPOC Pipeline yielded an additional planet candidate with a period of 7.8 days (TOI 186.02).

We used the 2-minute target pixel data for our analysis. The target is on the edge of the camera, where the point spread function is triangular in shape. After identifying the two transits, we tried improving the light curve precision by extracting light curves from the pub-

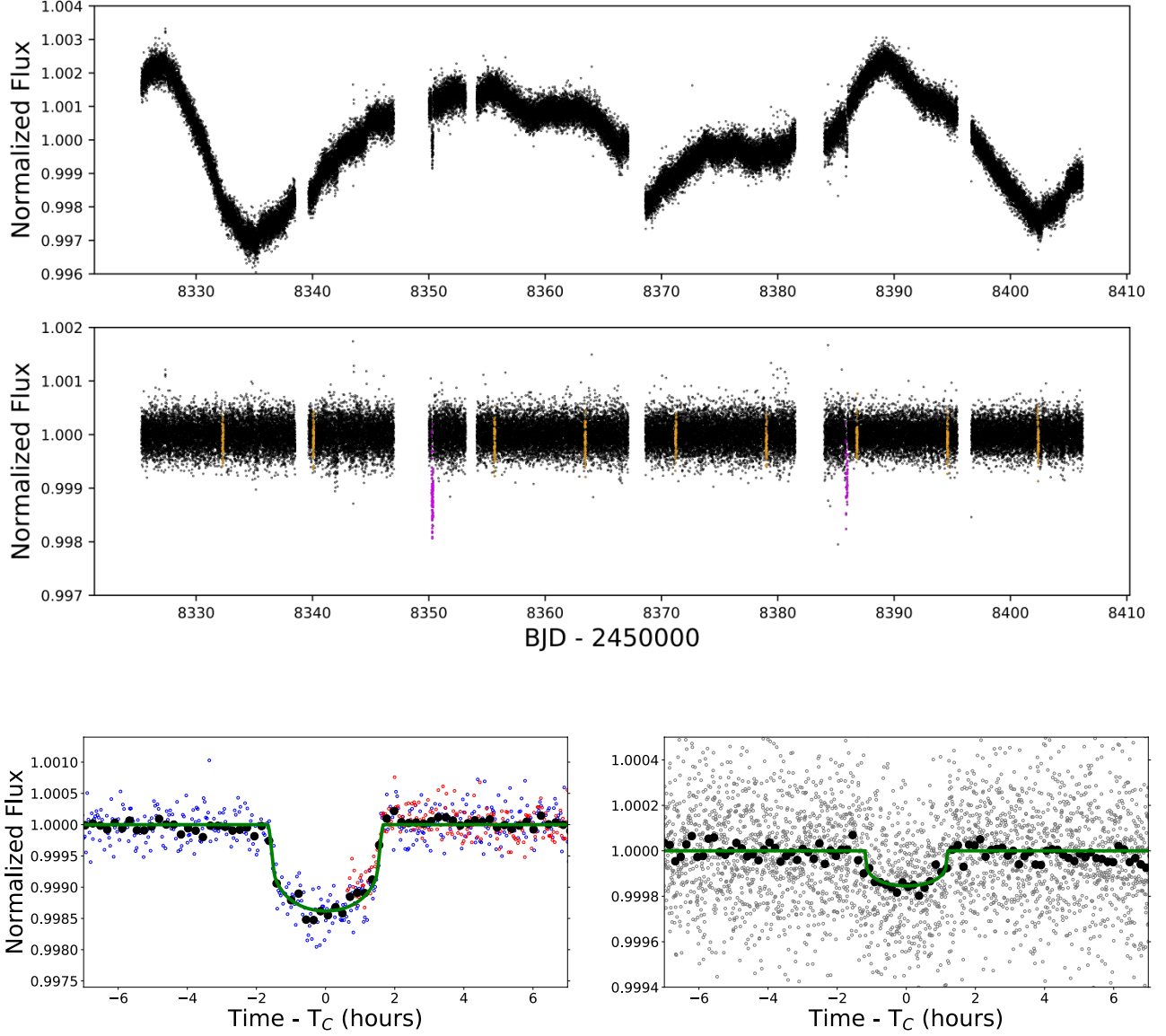


Figure 1. *TESS* photometry of HD 21749. *Top:* Raw light curve spanning three sectors. *Middle:* Light curve after spline was applied (see text for details). Transits of HD 21749b are shown in magenta, and transits of TOI 186.02 are shown in orange. *Bottom, left:* Phase-folded transits of HD 21749b, using a period of 35.61 days. The full transit from sector 1 is shown in blue, and the partial transit from sector 3 in red. *Bottom, right:* Phase-folded transits of TOI 186.02, using a period of 7.79 days. In both bottom plots, the binned light curves and best-fit transit models are plotted with black points and green lines, respectively.

licly available target pixel stamps using different photometric apertures (circles as well as irregular pixel boundaries). We then high-pass-filtered the raw light curve by fitting a basis spline with knots spaced by 0.3 days, after excluding both 3σ outliers and data obtained during and immediately surrounding transits (Vanderburg & Johnson 2014). The final 2-minute cadence light curve has an RMS of 240 ppm.

Care must be taken to rule out false positives that could masquerade as planet candidates. A giant star (HIP 16068/TIC 279741377; $R_* = 3.15^{+0.12}_{-0.09} R_\odot$) is

present $22''$ from HD 21749. The excellent period match between the transits and the HD 21749 RVs rule out this neighboring star as the source of the TOI 186.01 transit signals. Both planet candidates on HD 21749 also pass the false positive tests performed on the *TESS* photometry: there is no evidence of secondary eclipses or differences between the transit depths of particular planet candidates, nor any detectable motion of the centroid of the star on the detector during the transit events.

However, we cannot completely rule out the neighboring giant star as the source of the TOI 186.02 transit sig-

nals. If TOI 186.02 transits the giant star, it would have to be a Jupiter-sized object since the transit events have a low impact parameter (and are thus highly unlikely to be due to a grazing eclipsing binary). The presence of the neighboring star also warrants correcting the transit depths for dilution (see 3.2).

2.2. VLT NaCo Imaging

To test for nearby stellar companions, which could dilute the light curve and bias the measured planetary radius, we use archival data from the VLT/NaCo instrument (Lenzen et al. 2003; Rousset et al. 2003) collected in 2005 under program 076.C-0762(A). We use the first set of ten saturated frames collected on 2005-11-29, since the flux transmission degrades in the second set of ten frames. We additionally used two unsaturated frames, taken immediately before and after these saturated frames, to calibrate the flux of companions to which we are sensitive. The data were collected in the SDI mode with a Wollaston prism. This separates the light into four beams that are imaged through different wavelength filters. It includes multiple field orientations, allowing for an SDI+ADI analysis (see Schnupp et al. 2010). For simplicity, we use only the $1.6\mu\text{m}$ data in the upper left quadrant of the chip, and simply co-add the aligned data rather than performing a full ADI/SDI analysis.

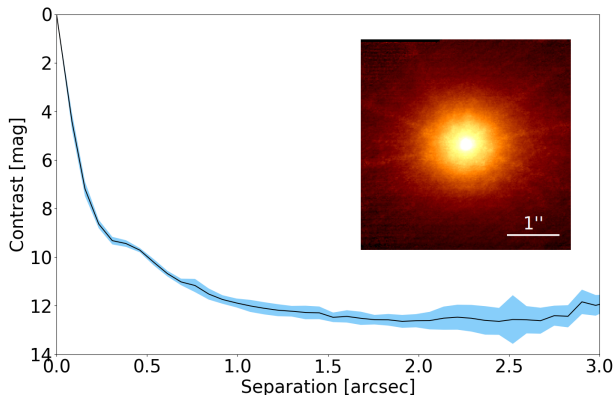


Figure 2. Sensitivity curve for the high-resolution AO imaging of the target with VLT/NaCo. The inset image is $4'' \times 4''$. No companions are detected within the field of view, and the target appears single to the limit of the imaging resolution.

Each saturated frame consists of 28 exposures of 6 seconds, corresponding to a total integration time of 1680s. We first subtract a sky background where a matching integration time is available, and a dark frame otherwise. The data are then cropped to the relevant section of the chip, and flat-fielded. The stellar position is aligned between frames, and frames derotated to align the north angle. Frames are then median combined to create a final image of the target. To determine the sensitivity of

this image, we inserted scaled copies of the unsaturated PSF, and recovered these with standard aperture photometry. A sensitivity curve is shown in Figure 2, along with a high angular resolution image of HD 21749. The target appears single to the resolution of these images, with no companions detected within the field of view, which extends to at least $2''$ from the target in every direction. Beyond this separation *Gaia* is sensitive to companions ~ 6 mag fainter than the host, and a companion of this magnitude would change the measured planet radius by 0.2%. We conclude that the measured radius of HD 21749b is unbiased by nearby stars.

2.3. HARPS Spectroscopy

We collected 59 observations of HD 21749 taken with the High-Accuracy Radial-velocity Planet Searcher HARPS (Mayor et al. 2003) on the ESO 3.6m telescope at La Silla Observatory in Chile. These observations are publicly available on the ESO Science Archive Facility. We extracted precision radial velocities from these $R \sim 115,000$ spectra and utilized them to both rule out a close-in binary as the origin of the transit signal, and to measure the mass of HD 21749b.

Of the 59 HARPS observations, 55 were obtained by the original HARPS guaranteed time observation (GTO) to search for planets between 2003 and 2009, and four measurements were obtained by another program in 2016. The data taken in 2016 have slightly different coordinates and proper motion, and the RVs were extracted using a template for a different spectral type compared to the data obtained by the HARPS GTO. We homogenized all the observations to account for these differences, and re-reduced all the data using the latest HARPS pipeline¹. In addition, these latest observations were gathered after an upgrade to the instrument that involved a change of some optical fibres (in May 2015, Lo Curto et al. 2015). This modification induced a few m/s offset in RV that is dependent on the stellar spectral type. It is difficult to model this offset, and the best option so far is to fit for an offset between the HARPS data taken before and after this fibre change (see 3.2).

2.4. PFS Spectroscopy

The second PRV data set presented in this work comes from the iodine-fed Planet Finder Spectrograph (PFS Crane et al. 2006, 2008, 2010) on the 6.5m Magellan II telescope at Las Campanas Observatory in Chile. HD 21749 was observed with PFS, with somewhat irregular sampling, as part of the long-term Magellan Planet Search Program between January 2010 and Oc-

¹ The consistently-reduced set of HARPS RVs can be obtained through the DACE platform: dace.unige.ch.

tober 2018, for a total of 48 radial velocities (45 epochs). We then began a high-cadence observing campaign purposely for *TESS* follow-up in December 2018, adding 34 more velocities (nine more epochs). The iodine data prior to 2018 were taken through a $0.5''$ slit resulting in $R \sim 80,000$, and post-2018 were taken through $0.3''$ slit, resulting in $R \sim 130,000$; the iodine-free template was taken through the $0.3''$ slit. The pre-2018 and 2018 data are separated in the orbital fitting because the PFS detector and observing strategy changed in Feb. 2018 and the jitter in the 2018 observations is significantly lower. Exposure times ranged from ~ 150 s to ~ 600 s, depending on the conditions, resulting in S/N of ~ 100 to 200. All PFS data are reduced with a custom IDL pipeline that flat fields, removes cosmic rays, and subtracts scattered light. Further details about the iodine-cell RV extraction method can be found in [Butler et al. \(1996\)](#).

3. ANALYSIS AND RESULTS

3.1. Stellar Parameters

We performed a fit to the broadband spectral energy distribution (SED), following the methodology described in [Stassun et al. \(2018, 2017\)](#); [Stassun & Torres \(2016\)](#). We adopted the fluxes published in all-sky photometric catalogs: *Tycho-2* $B_T V_T$, *2MASS* JHK_S , and *WISE*1–4. These flux measurements span the wavelength range 0.4 – $22 \mu\text{m}$. We assumed solar metallicity based on values in the PASTEL catalog ([Soubiran et al. 2016](#)), and we fit Kurucz atmosphere models with the free parameters being the effective temperature, the overall flux normalization, and the extinction, the latter limited to the maximum line-of-sight value from the dust maps of [Schlegel et al. \(1998\)](#). The resulting SED fit has a reduced $\chi^2 = 3.4$, $T_{\text{eff}} = 4640 \pm 100$ K, $A_V = 0.14^{+0.00}_{-0.04}$, $F_{\text{bol}} = 2.43 \pm 0.11 \times 10^{-8} \text{ erg s}^{-1} \text{ cm}^{-2}$. With the *Gaia* DR2 parallax corrected for systematic offset from [Stassun & Torres \(2018\)](#), this gives $R_\star = 0.695 \pm 0.030 R_\odot$. We can also estimate the stellar mass from the empirical relations of [Torres et al. \(2010\)](#), which gives $M_\star = 0.73 \pm 0.07 M_\odot$. Together with the stellar radius, this then provides an empirical estimate of the stellar mean density, $\rho_\star = 3.09 \pm 0.23 \text{ g cm}^{-3}$. The top section of Table 1 lists the stellar parameters.

3.2. Joint Photometry and Radial Velocity Fit

We performed two independent analyses that jointly fitted the *TESS* photometry with the HARPS and PFS RVs, using a 2-planet model with a long-term trend ($\dot{\gamma}$). We used *EXOFASTv2* ([Eastman 2017](#); [Eastman et al. 2013](#)) and *allesfitter* ([Güenther & Daylan, in prep.](#)). *EXOFASTv2* is based on a differential evolution Markov Chain Monte Carlo algorithm that uses error scaling and includes integrated isochrone and SED models to optionally constrain the stellar properties. *allesfitter* is

an inference framework that unites the packages *ellc* (light curve and RV models; [Maxted 2016](#)), *dynesty* (static and dynamic nested sampling; <https://github.com/joshspeagle/dynesty>), *emcee* (MCMC sampling; [Foreman-Mackey et al. 2013](#)) and *celerite* (GP models; [Foreman-Mackey et al. 2017](#)) to model systematic noise in the photometry. Here, we used *allesfitter* with nested sampling instead of MCMC.

We also fitted for constant offsets and jitter terms (added in quadrature to the instrumental uncertainties) for each of the four RV data sets we use: HARPS 1 (pre-upgrade), HARPS 2 (post-upgrade), PFS 1 (pre-upgrade), PFS 2 (post-upgrade).

We used the stellar mass, radius, metallicity and temperature values listed in 3.1 as Gaussian priors for both analyses (we did not use any of the relations provided with *EXOFASTv2* for constraining stellar parameters). We also fit for dilution of the transit signal due to the neighboring star, for which we used the contamination ratio from TIC V7 ([Stassun et al. 2017](#)) and 10% of its value as a Gaussian prior. We did not use any other Gaussian priors for either analysis. We note that *EXOFASTv2* determines and uses quadratic limb darkening coefficients interpolated from the Claret tables for *TESS* ([Claret 2017](#)), while *allesfitter* fits a linear limb darkening coefficient to the *TESS* photometry.

The best-fit parameter values are consistent between our two independent analyses. To make it easier to reproduce our results, we report in this work the values from the *EXOFASTv2* fit (see Table 1). We also report RV planetary parameters for the 7.8-day planet candidate, TOI 186.02, assuming it orbits HD 21749. However, the RV semi-amplitude is consistent with 0. We set a 3σ upper limit of ~ 1.7 m/s on the semi-amplitude of this planet candidate.

We note that an independent analysis of the RV measurements using RadVel ([Fulton et al. 2018](#)) with the periods fixed to 35.608 and 7.7882 days and T_c for each planet fixed to the *TESS*-determined values, gives results for K , e and ω that are fully consistent with those in Table 1.

Finally, as an experiment before the *TESS* sector 3 data became available, we performed a joint analysis of the sector 1 transit together with the HARPS RVs. The period determination of this fit was driven by the RVs, and the transit only poorly constrained the time of inferior conjunction because of the long baseline between the RV and *TESS* measurements. Notably, the fit preferred a higher eccentricity (which is no longer allowed when including the second transit and the PFS RVs), and a time of periastron passage offset by 10 days from the true value. The best-fit period was also shorter and the best-fit mass was higher than the values obtained when using both transits.

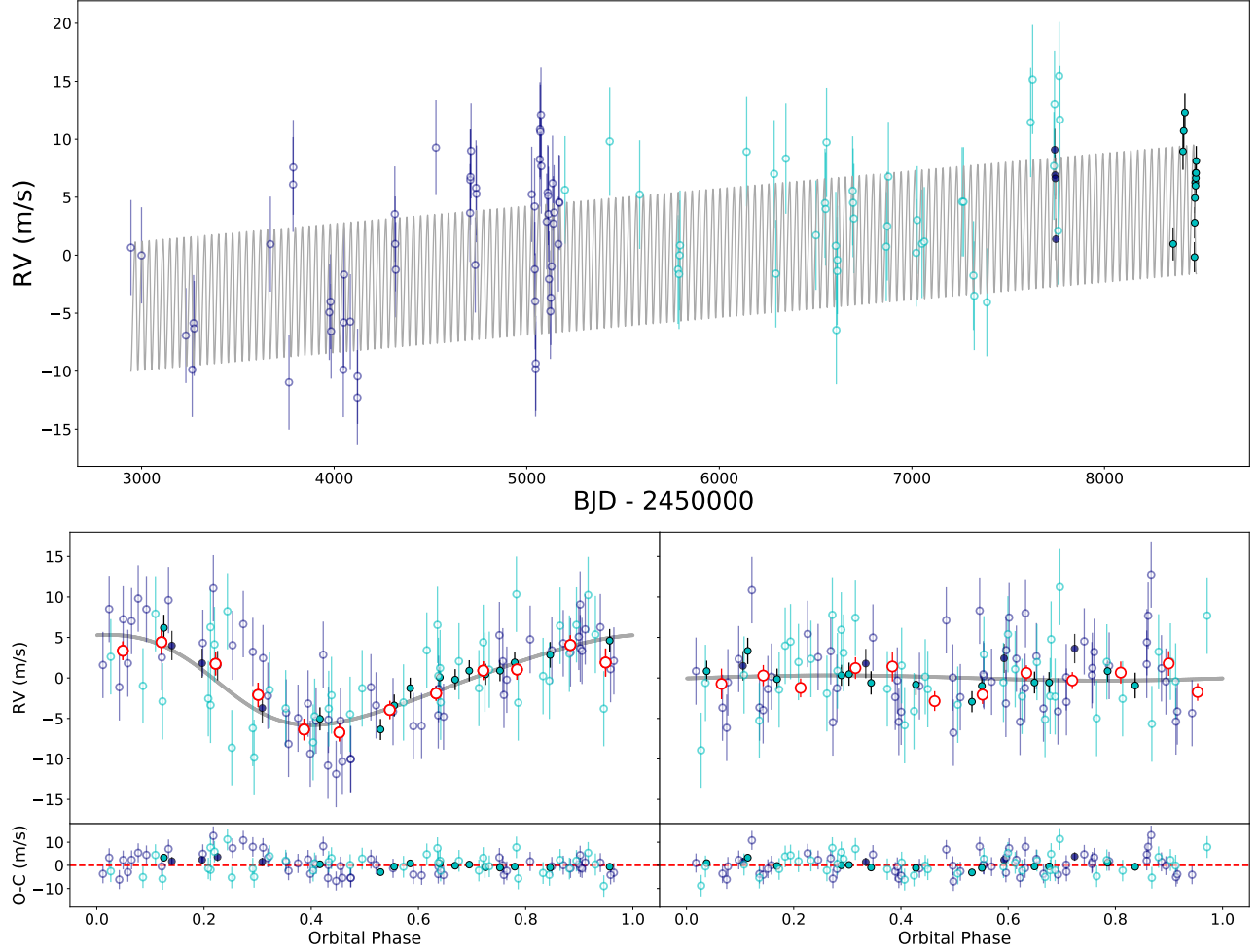


Figure 3. Relative RV measurements and best-fit models for HD 21749. *Top:* Complete time series including HARPS pre-upgrade (dark blue open circles), HARPS post-upgrade (dark blue points), PFS pre-upgrade (cyan open circles), and PFS post-upgrade (cyan points) data. The error bars are the quadrature sum of the instrument jitter terms and the measurement uncertainties for all RVs. The best-fit constant offsets have been subtracted, and the gray line shows the best-fit 2-planet RV model. *Bottom:* Phase-folded radial velocities using periods of 35.61 days for planet b (left) and 7.788 days for planet c (right), with residuals shown below. Point colors are as in the top panel, with the addition of red open circles showing the average velocities binned in 0.073 intervals of orbital phase. Each planet’s best-fit model is shown with a gray line, with the Keplerian orbital model for the other planet and the long term trend subtracted.

Our findings underline the need for at least two transits (not necessarily all from *TESS*) to confirm a *TESS* planet and determine its properties adequately. A single transit is insufficient, even if RVs are available.

3.3. Stellar Activity

As mentioned in 2.1, the $\log(R_{HK})$ value for HD 21749 suggests a stellar rotation period of 34.5 ± 7 days (Mamajek & Hillenbrand 2008). We investigate this further by extracting S_{HK} and H_{α} indices from the HARPS and PFS (pre-upgrade only) spectra. Figure 4 shows Lomb-Scargle periodograms of these indices (second and third panels from the top). In the 10 to 100-day range, the highest peak in both of these HARPS activity indicators corresponds to 37.19 days, which we attribute to the rotation of the star. We do not see significant power at

the period of HD 21749b.

We also obtained Kilodegree Extremely Little Telescope (KELT; Pepper et al. 2004) photometry of HD 21749. The star has been monitored by KELT as part of their long-term transit survey of bright stars. The KELT light curve for HD 21749 spans ~ 3.3 years, contains 7848 individual points (taken between February, 2010 and June, 2013), and has an RMS of ~ 0.0098 mag. A Lomb-Scargle periodogram of the KELT photometry finds the most significant peak at a period of 38.954 days (see bottom panel of Figure 4).

More data will help to pin down the stellar rotation period more precisely. The existing photometric and spectroscopic data sets suggest that the stellar rotation period is longward of the planet period. Importantly, the RV periodogram (top panel of Figure 4) shows the

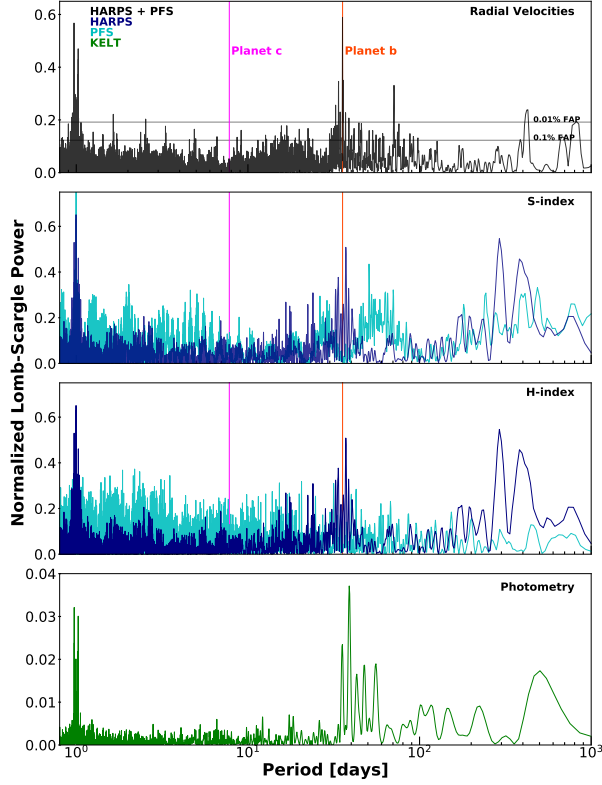


Figure 4. Lomb-Scargle periodograms of, from top to bottom: the complete set of RVs, the S_{HK} index, the H_{α} index and the KELT photometry. Red and magenta lines mark the periods of HD 21749b and TOI 186.02, respectively.

strongest peak at 35.6 days (the period of HD 21749b) but does not show significant (above 0.01% FAP) power in the 37 to 39-day period range.

Nevertheless, we employ equation 2 of [Vanderburg et al. \(2016\)](#) to estimate the magnitude of systematic errors due to the stellar variability ($\sigma_{s,RV}$) that could affect the RV signals of HD 21749b and TOI 186.02. We use the standard deviation of the raw *TESS* light curve ($\sigma_{s,TESS} = 0.0013$) rather than its peak-to-peak amplitude ($Fpp_{s,TESS}$), and $v_{\sin i} = 1.04$ km/s (derived from the HARPS spectra) to obtain $\sigma_{s,RV} \approx 1.3$ m/s.

Therefore, while we do not expect the RV signal of HD 21749b to be strongly affected by stellar variability, the uncertainties on the K values reported in Table 1 could be underestimated.

4. DISCUSSION AND CONCLUSION

In this Letter we announce the discovery and confirmation of HD 21749b, the second *TESS* Level-1 planet ($R_P < 4 R_{\oplus}$ and a measured mass) to date, and the longest-period *TESS* planet confirmed so far. We also report the discovery of an Earth-sized planet candidate around HD 21749 which, if confirmed, would become the smallest *TESS* planet found to date.

HD 21749b is a $2.8 R_{\oplus}$ planet. Using HARPS and PFS

RVs, we measured its mass at $23.20^{+2.13}_{-1.91} M_{\oplus}$. Its density of $5.7^{+1.7}_{-1.4}$ g/cm³ makes it one of the three densest planets with a mass above $15 M_{\oplus}$. The other two are Kepler-131b (M_P of $16.1 \pm 3.5 M_{\oplus}$ and ρ_P of 6.0 ± 2.0 g/cm³; [Marcy et al. 2014](#)) and K2-66b (M_P of $21.3 \pm 3.6 M_{\oplus}$, ρ_P of 7.8 ± 2.7 g/cm³; [Sinukoff et al. 2017](#)). Both Kepler-131b and K2-66b have densities consistent with a rocky composition, but they are also less massive than HD 21749b. On the other hand, the density of HD 21749b indicates it is likely surrounded by a substantial atmosphere. By measuring the density of these three planets (and other similar planets that *TESS* may find) more precisely, we can begin to observationally constrain the maximum core mass a planet can reach during its formation before accreting a volatile envelope.

According to the transmission spectroscopy metric (TSM) of ([Kempton et al. 2018](#)), HD 21749b is not an ideal target for atmospheric characterization with the JWST. However, the TSM is based on 10 hours of JWST observing time. *TESS* sub-Neptunes transiting bright K dwarfs and with relatively low equilibrium temperature may be scarce. Therefore, HD 21749b could easily warrant more observing time, particularly to search for species expected in cooler planets (i.e. methane). It may also be possible to measure HD 21749b’s spin/orbit obliquity via the Rossiter McLaughlin effect with either ESPRESSO ([Pepe et al. 2010](#)) or precise spectrographs planned for the Extremely Large Telescopes currently in development.

TOI 186.02 is an Earth-sized planet candidate. If we assume it orbits HD 21749, its mass is expected to be $\sim 2.5 M_{\oplus}$ according to the M-R relations of [Ning et al. \(2018\)](#) (though Earth-sized planets with mass of $1 M_{\oplus}$ are known to exist). This would give rise to a RV semi-amplitude of ~ 1.0 m/s, a challenging measurement for the RV spectrographs presented here, but perhaps more feasibly measured with a dedicated VLT/ESPRESSO campaign.

Finally, we emphasize that this work used mainly existing spectroscopic and photometric data, publicly available (as for [Huang et al. 2018a](#) and [Vanderspek et al. 2018](#)) or generously contributed by multiple ongoing surveys, to confirm and characterize the planet presented in this work. We postulate that this approach has the potential to be successful for other *TESS* planet candidates as well.

An independent analysis of archival HARPS RVs of HD 21749 has also been reported (Trifonov et al., arXiv:1812.04501). Our paper differs in scope in that we confirm HD 21749b using *TESS* photometry, HARPS and PFS RVs, and we report a new planet candidate.

Moreover, we investigate the stellar activity and find evidence that the stellar rotation period does not coincide with the period of the newly confirmed planet.

Funding for the *TESS* mission is provided by NASA’s Science Mission directorate. We acknowledge the use of public *TESS* Alert data from pipelines at the *TESS* Science Office and at the *TESS* Science Processing Operations Center. This paper includes data collected by the *TESS* mission, which are publicly available from the Mikulski Archive for Space Telescopes (MAST). This work is based on observations collected at the European Southern Observatory under ESO programmes 076.C-0762(A), 096.C-0499(A), 183.C-0972(A) and 072.C-0488(E). DD and JT acknowledge support for this work provided by NASA through Hubble Fellowship grants HST-HF2-51372.001-A and HST-HF2-51399.001-A awarded by the Space Telescope Science Institute, which is operated by the Association of Universities for Research in Astronomy, Inc., for NASA, under contract NAS5-26555. MNG, JB, and CXH ac-

knowledge support from MITs Kavli Institute as Torres postdoctoral fellows. AV’s work was performed under contract with the California Institute of Technology (Caltech)/Jet Propulsion Laboratory (JPL) funded by NASA through the Sagan Fellowship Program executed by the NASA Exoplanet Science Institute. JER was supported by the Harvard Future Faculty Leaders Postdoctoral fellowship. XD acknowledges support from the Branco Weiss Fellowship–Society in Science.

Software: *EXOFASTv2* (Eastman 2017), *allesfitter* (Gunther & Daylan, in prep.), *ellc* (Maxted 2016), *dynesty* (<https://github.com/joshspeagle/dynesty>), *emcee* (Foreman-Mackey et al. 2013), *celerite* (Foreman-Mackey et al. 2017), *RadVel* (Fulton et al. 2018)

Facilities: *TESS*, ESO 3.6 m: HARPS, Magellan:Clay (Planet Finder Spectrograph), VLT: NACO, KELT

REFERENCES

- Barclay, T., Pepper, J., & Quintana, E. V. 2018, ArXiv e-prints, arXiv:1804.05050
- Boro Saikia, S., Marvin, C. J., Jeffers, S. V., et al. 2018, *A&A*, 616, A108
- Butler, R. P., Marcy, G. W., Williams, E., et al. 1996, *Publications of the Astronomical Society of the Pacific*, 108, 500
- Claret, A. 2017, *A&A*, 600, A30
- Crane, J. D., Shectman, S. A., & Butler, R. P. 2006, in *Society of Photo-Optical Instrumentation Engineers (SPIE) Conference Series*, Vol. 6269, 626931
- Crane, J. D., Shectman, S. A., Butler, R. P., et al. 2010, in *Ground-based and Airborne Instrumentation for Astronomy III*, Vol. 7735, 773553
- Crane, J. D., Shectman, S. A., Butler, R. P., Thompson, I. B., & Burley, G. S. 2008, in *Society of Photo-Optical Instrumentation Engineers (SPIE) Conference Series*, Vol. 7014, *Ground-based and Airborne Instrumentation for Astronomy II*, 701479
- Dragomir, D., Matthews, J. M., Eastman, J. D., et al. 2013, *ApJL*, 772, L2
- Eastman, J. 2017, *EXOFASTv2: Generalized publication-quality exoplanet modeling code*, *Astrophysics Source Code Library*, , ascl:1710.003
- Eastman, J., Gaudi, B. S., & Agol, E. 2013, *PASP*, 125, 83
- Foreman-Mackey, D., Agol, E., Angus, R., & Ambikasaran, S. 2017, *AJ*, 154, 220
- Foreman-Mackey, D., Hogg, D. W., Lang, D., & Goodman, J. 2013, *PASP*, 125, 306
- Fressin, F., Torres, G., Charbonneau, D., et al. 2013, *ApJ*, 766, 81
- Fulton, B. J., Petigura, E. A., Blunt, S., & Sinukoff, E. 2018, *PASP*, 130, 044504
- Fulton, B. J., Petigura, E. A., Howard, A. W., et al. 2017, ArXiv e-prints, arXiv:1703.10375
- Gillon, M., Triaud, A. H. M. J., Demory, B.-O., et al. 2017, *Nature*, 542, 456
- Howard, A. W., Marcy, G. W., Bryson, S. T., et al. 2012, *ApJS*, 201, 15
- Huang, C. X., Shporer, A., Fausnaugh, M., et al. 2018a, *AAS Journals*, submitted
- Huang, C. X., Burt, J., Vanderburg, A., et al. 2018b, *ApJ*, 868, L39
- Jenkins, J. M. 2017, *Kepler Data Processing Handbook: Overview of the Science Operations Center*, Tech. rep.
- Jenkins, J. M., Chandrasekaran, H., McCauliff, S. D., et al. 2010, in *Proc. SPIE*, Vol. 7740, *Software and Cyberinfrastructure for Astronomy*, 77400D
- Jenkins, J. M., Twicken, J. D., McCauliff, S., et al. 2016, in *Proc. SPIE*, Vol. 9913, *Software and Cyberinfrastructure for Astronomy IV*, 99133E
- Kempton, E. M.-R., Bean, J. L., Louie, D. R., et al. 2018, *PASP*, 130, 114401
- Lenzen, R., Hartung, M., Brandner, W., et al. 2003, in *Proc. SPIE*, Vol. 4841, *Instrument Design and Performance for Optical/Infrared Ground-based Telescopes*, ed. M. Iye & A. F. M. Moorwood, 944–952
- Lo Curto, G., Pepe, F., Avila, G., et al. 2015, *The Messenger*, 162, 9
- Lovis, C., Mayor, M., Bouchy, F., et al. 2009, in *IAU Symposium*, Vol. 253, *Transiting Planets*, ed. F. Pont, D. Sasselov, & M. J. Holman, 502–505
- Mamajek, E. E., & Hillenbrand, L. A. 2008, *ApJ*, 687, 1264
- Marcy, G. W., Isaacson, H., Howard, A. W., et al. 2014, *ApJS*, 210, 20
- Maxted, P. F. L. 2016, *A&A*, 591, A111
- Mayor, M., Pepe, F., Queloz, D., et al. 2003, *The Messenger*, 114, 20
- Ning, B., Wolfgang, A., & Ghosh, S. 2018, ArXiv e-prints, arXiv:1811.02324
- Pepe, F. A., Cristiani, S., Rebolo Lopez, R., et al. 2010, in *Proc. SPIE*, Vol. 7735, *Ground-based and Airborne Instrumentation for Astronomy III*, 77350F

- Pepper, J., Gould, A., & Depoy, D. L. 2004, in American Institute of Physics Conference Series, Vol. 713, The Search for Other Worlds, ed. S. S. Holt & D. Deming, 185–188
- Ricker, G. R., Winn, J. N., Vanderspek, R., et al. 2015, *Journal of Astronomical Telescopes, Instruments, and Systems*, 1, 014003
- Rousset, G., Lacombe, F., Puget, P., et al. 2003, in *Proc. SPIE*, Vol. 4839, Adaptive Optical System Technologies II, ed. P. L. Wizinowich & D. Bonaccini, 140–149
- Schlegel, D. J., Finkbeiner, D. P., & Davis, M. 1998, *ApJ*, 500, 525
- Schnupp, C., Bergfors, C., Brandner, W., et al. 2010, *A&A*, 516, A21
- Sinukoff, E., Howard, A. W., Petigura, E. A., et al. 2017, *AJ*, 153, 271
- Soubiran, C., Le Campion, J.-F., Brouillet, N., & Chemin, L. 2016, *A&A*, 591, A118
- Stassun, K. G., Corsaro, E., Pepper, J. A., & Gaudi, B. S. 2018, *AJ*, 155, 22
- Stassun, K. G., & Torres, G. 2016, *AJ*, 152, 180
- . 2018, *ApJ*, 862, 61
- Stassun, K. G., Oelkers, R. J., Pepper, J., et al. 2017, *ArXiv e-prints*, arXiv:1706.00495
- Sullivan, P. W., Winn, J. N., Berta-Thompson, Z. K., et al. 2015, *ApJ*, 809, 77
- Torres, G., Andersen, J., & Giménez, A. 2010, *A&A Rv*, 18, 67
- Vanderburg, A., & Johnson, J. A. 2014, *PASP*, 126, 948
- Vanderburg, A., Plavchan, P., Johnson, J. A., et al. 2016, *MNRAS*, 459, 3565
- Vanderspek, R., Huang, C. X., Vanderburg, A., et al. 2018, *arXiv e-prints*, arXiv:1809.07242
- Villanueva, Jr., S., Dragomir, D., & Gaudi, B. S. 2018, *ArXiv e-prints*, arXiv:1805.00956

Table 1. Median values and uncertainties for the HD 21749 system

Parameter	Value
Catalogue Stellar Information:	
R.A. Right Ascension (h:m:s; J2015.5)	03:27:00.045
Dec Declination (d:m:s; J2015.5)	-63:30:00.60
λ Ecliptic longitude (deg)	352.8828
β Ecliptic latitude (deg)	-73.8346
HD ID Henry Draper Catalogue ID	21749
TIC ID <i>TESS</i> Input Catalogue ID	279741379
TOI ID <i>TESS</i> Object of Interest ID	186.01
Photometric Stellar Properties:	
V mag Relative V-band magnitude	8.1
<i>TESS</i> mag Relative <i>TESS</i> -band magnitude	6.95
Stellar Parameters:	
D Distance (pc).....	16.33 ± 0.007
M_* Mass (M_\odot)	0.73 ± 0.07
R_* Radius (R_\odot)	0.695 ± 0.030
L_* Luminosity (L_\odot).....	0.20597 ± 0.00016
ρ_* Density (cgs).....	$3.03^{+0.50}_{-0.47}$
$\log g$ Surface gravity (cgs)	$4.613^{+0.052}_{-0.061}$
T_{eff} Effective Temperature (K).....	4640 ± 100
[Fe/H] Metallicity (dex)	0.003 ± 0.060
MCMC Fit <i>TESS</i> Bandpass Wavelength Parameters:	
u_1 linear limb-darkening coeff	0.524 ± 0.046
u_2 quadratic limb-darkening coeff	$0.185^{+0.047}_{-0.048}$
A_D Dilution from neighboring stars	0.152 ± 0.099
MCMC Fit Telescope Parameters:	
$\dot{\gamma}$ RV slope (m/s/day).....	$0.00152^{+0.00069}_{-0.00067}$
$\gamma_{\text{rel},1}$ Relative RV Offset HARPS 1 (m/s) .	$59609.08^{+0.66}_{-0.65}$
$\gamma_{\text{rel},2}$ Relative RV Offset HARPS 2 (m/s) .	59619.3 ± 3.1
$\gamma_{\text{rel},3}$ Relative RV Offset PFS 1 (m/s).....	$-4.5^{+0.62}_{-0.61}$
$\gamma_{\text{rel},4}$ Relative RV Offset PFS 2 (m/s).....	-5.3 ± 3.0
$\sigma_{J,1}$ RV Jitter HARPS 1 (m/s).....	$4.09^{+0.46}_{-0.39}$
$\sigma_{J,2}$ RV Jitter HARPS 2 (m/s).....	$1.4^{+4.4}_{-1.4}$
$\sigma_{J,3}$ RV Jitter PFS 1 (m/s).....	$4.59^{+0.63}_{-0.52}$
$\sigma_{J,4}$ RV Jitter PFS 2 (m/s).....	$1.12^{+0.20}_{-0.18}$
MCMC Fit Planetary Parameters:	
P Period (days).....	35.6077 ± 0.0014
T_C Time of conjunction (BJD _{TDB}).....	$2458350.31233^{+0.00062}_{-0.00059}$
K RV semi-amplitude (m/s)	$5.68^{+0.4}_{-0.37}$
	HD 21749b
	TOI 186.02
	$7.78798^{+0.00034}_{-0.00040}$
	$2458332.29123^{+0.0021}_{-0.00092}$
	$0.32^{+0.46}_{-0.32}$

Table 1 continued

Table 1 (*continued*)

Parameter	Value	
$ecos\omega_*$	$-0.042^{+0.051}_{-0.050}$	—
$esin\omega_*$	$0.186^{+0.078}_{-0.084}$	—
i	$89.36^{+0.18}_{-0.12}$	$89.02^{+0.55}_{-0.42}$
R_P/R_*	$0.0378^{+0.0027}_{-0.0023}$	$0.01232^{+0.00097}_{-0.00087}$
Derived Planetary Parameters:		
e	$0.198^{+0.073}_{-0.077}$	—
ω_*	103^{+20}_{-16}	—
T_P	$2458351.14^{+1.5}_{-0.99}$	$2458332.29123^{+0.0021}_{-0.00092}$
a/R_*	$59.9^{+2.9}_{-3.2}$	21.7 ± 1.1
a	$0.1914^{+0.0056}_{-0.0061}$	$0.0695^{+0.0021}_{-0.0022}$
R_P	$2.836^{+0.258}_{-0.224}$	$0.9236^{+0.0897}_{-0.0773}$
T_{eq}	423^{+14}_{-13}	703^{+24}_{-22}
M_P	$23.20^{+2.13}_{-1.91}$	$0.7945^{+1.1441}_{-0.7945}$
τ	$0.0071^{+0.0020}_{-0.0015}$	$0.00152^{+0.00026}_{-0.00019}$
T_{14}	$0.1380^{+0.0019}_{-0.0016}$	$0.1067^{+0.0047}_{-0.0039}$
b	$0.55^{+0.11}_{-0.18}$	$0.37^{+0.14}_{-0.20}$
ρ_P	$5.7^{+1.7}_{-1.4}$	$5.3^{+9.1}_{-5.3}$
$logg_P$	$3.456^{+0.080}_{-0.084}$	$2.96^{+0.41}_{-3.2}$